Experimental strength characterisation of thin chemically pre-stressed glass based on laser-induced flaws

Abstract

The strength of chemically pre-stressed glass depends on the depth of surface flaws and the value of the pre-stress. So far, some research has been conducted on this topic; however, there were always uncertainties regarding the flaw depth and the pre-stress profile. Consequently, this research characterises the pre-stress profile using experimental methods. The latter include measuring the depth of layer (DoL) and the surface compressive pre-stress (C_S) with FSM-7000h and verifying the achieved DoL with the Na^+ and K^+ distribution through the thickness obtained from the SEM/EDS analysis. Results demonstrate that the amount of K decreases parabolically (second-order) to a certain value and then remains constant. Based on this observation and some boundary conditions, the equation of the pre-stress profile was obtained for thin chemically pre-stressed aluminosilicate glass (Falcon®) with 8h and 24h processing durations in molten salt at 460 ˚C. A non-strengthened glass (NSG) was also used as a reference for comparison. Then, three artificial laser-induced flaws with accurately controlled depths is tested by means of a clamp bender. The results of the strength tests demonstrated very low deviations in the failure stress. It was shown that even when the depth of the flaw is higher than the DoL, which means that the flaw tip enters the zone with the pre-tensile stress, there is still considerable resistance from the surrounding intact area. Furthermore, it was confirmed that the pre-stress strain energy for 24h processing is larger than for 8h, leading to more fragmentation after failure under a similar loading condition. Finally, it was found that the fracture toughness is not constant through the pre-stressed glass thickness, and it is dependent on the pre-stress profile with the peak value at the glass surface.

Keywords:

Chemically strengthened glass, Thin glass, Surface flaw, Laser ablation, Bending strength

1. Introduction

Tensile stress has always been a weak spot of glass. Several techniques have been used to increase the glass tensile capacity to overcome this issue. Strengthening is one of the most common techniques for this purpose. Strengthening can be implemented either thermally or chemically, in which pre-stressed layers are introduced on both sides of the glass (Kistler 1962; Lee, Rogers, and Woo 1965; Belis et al. 2019). In the thermal strengthening process, the glass is heated above the glass transition temperature, and subsequently quenched. In this way, the glass surfaces cool faster than the core, leading to the creation of residual compressive stress at the surfaces and tensile stress in the core (Bartenev 1948; Nielsen, Olesen, and Stang 2010; Nielsen et al. 2021). The depth of the compressive pre-stress region for the case of thermal strengthening is around 21% of the glass thickness. This relatively thick compressive pre-stress region reduces the risk of flaw penetration to the tensile region (Schwind et al. 2020; Zaccaria and Overend 2020). However, the magnitude of the pre-compressive stress is significantly lower than that of chemically pre-stressed glass (Zaccaria et al. 2021). There are different terminologies in the literature to describe chemically pre-stressed glass, such as strengthened glass, toughened glass, and tempered glass. Although all of them can be correct from a certain perspective, we believe that the terms “chemically pre-stressed glass” and “chemically strengthened glass (CSG)” are best expressing the manufacturing process and the final product. CSG as a thermally activated diffusion process is typically produced by immersion of glass into a molten salt bath (KNO_3), whereby the larger ions in the salt (K^+) replace the smaller ions (Na^+) in the glass via an ion exchange process (Nordberg et al. 1964; Tyagi and Varshneya 1998; Gy 2008; Karlsson, Jonson, and Stålhandske 2010; Terakado et al. 2020).The

longer the glass is immersed, the larger the depth over which the ion exchange takes place, i.e. the so-called depth of layer (DoL) (Jiang et al. 2013). However, the compressive pre-stress does not increase steadily by increasing the immersion time because of the stress relaxation effect (Sane and Cooper 1987; Seaman et al. 2014). Therefore, chemically pre-stressing allows flexibility in tuning of the compressive pre-stress and DoL depending on the application. Nevertheless, the compressive pre-stress increases the strength of glass significantly (Macrelli 2018).

Glass strength is, to a large extent, determined by the most critical flaw on its surface. Since there are typically many random flaws with different locations, depths, and orientations on the glass, a high variation in strength values is expected. That is why usually a stochastic approach needs to be followed to analyze the data. However, if we can generate a flaw with well-known geometry and orientation from which fracture occurs, the glass strength as a result of that specific critical flaw can be determined with minimal statistical uncertainty. In this way, investigating the effect of other factors becomes much easier. To turn this deterministic approach into reality, good control over the flaw creation process is required.

So far, two methods have been used to create artificial flaws. The first method is using an indenter with direct contact to the glass (Glaesemann, Jakus, and Ritter 1987; Schneider, Schula, and Weinhold 2012; Moayedi and Wondraczek 2017; Bensaid et al. 2018; Varshneya et al. 2021). To achieve the best result, optimizing the indenter's corresponding parameters, velocity and normal load is required. However, due to the brittleness of glass, appearance of lateral/median cracks and chippings around the main flaw is almost inevitable. These undesirable flaws can affect the glass strength and decrease the accuracy of the results. Another bottleneck is the repeatability of the method considering the variability of the contact based method. To tackle this issue, a second method was used to create a wide variety of surface flaws with very good control over the flaw

depth, which is non-contact and laser-based (Nategh et al. 2021a; Nategh et al. 2021b). The very low deviation in the failure load values obtained based on four point bending tests was a clear indication of the reliability and repeatability of the method.

Putting effort into creating accurate artificial flaws without performing an accurate strength test is worthless. There are several methods for testing (thick) glass, among which four-point bending (EN 1288-3 2000; ASTM C158-02 2017) and co-axial double rings tests (EN 1288-2 2000; EN 1288-5 2000; ASTM C1499-19 2019) are the most common methods. However, these tests are not appropriate for thin glass (Maniatis, Nehring, and Siebert 2016). Santos et al. (2018) experimentally and numerically investigated four-point bending and buckling tests for determining the strength of thin glass. The drawback of a four-point bending test is that the thin glass becomes geometrically nonlinear due to the high deformation and the high strength obtained during the strengthening process. It was also shown that the buckling test is imperfect due to several failures from the location of the support as a consequence of stress concentration in the roller slit. Therefore, a tensile test was proposed, which was investigated numerically and seemed promising, but unfortunately, there was no experimental setup/result confirming the numerical analysis (Neugebauer 2016). Another approach for testing thin glass is bending it with a constant radius in which a bending moment is applied on the straight opposite edges (Zaccaria et al. 2022). The bending moment can be distributed uniformly and constantly by a precise movement of two applying moment arms (see section 2.3).

In this publication, the strength of thin chemically pre-stressed aluminosilicate glass (Falcon®) is studied based on the laser-induced artificial flaw method in combination with a dedicated clamp bender setup. Both annealed and chemically strengthened (with two different DoLs) Falcon glass with the same dimension were investigated to better understand the effect of strengthening on the

glass strength. After obtaining the pre-stress profiles with the help of FSM 7000h and SEM/EDS analysis, a picosecond laser with a wavelength of 532 nm was employed to create flaws with three different depths chosen based on the DoL of the strengthened glasses. The same laser but with a slight difference in the wavelength was used previously to realize artificial flaws in annealed soda-lime silica glass (Nategh, Missinne, et al. 2021a). In the last step, the clamp bender setup designed by AGC was used successfully for the strength measurement (Zaccaria et al. 2022).

2. Materials and methods

2.1. Glass

Aluminosilicate thin glass (Falcon®) with three different processing conditions is used, all having the same dimensions (100*50*0.5 mm): Type 1) chemically strengthened during 24 hours (CSG 24h), type 2) chemically strengthened during 8 hours (CSG 8h), and type 3) non-strengthened glass (NSG). CSG glass was submersed in a bath containing a potassium salt at 460 °C.

To verify the glass composition, a scanning electron microscope (SEM) coupled with an energy-dispersive X-ray spectroscopy (EDS) system is employed. EDS analysis yields the estimated material composition over a depth of 1—2 μm from the surface, and therefore the glass cross-section was inspected. Before EDS analysis, a cross-sectioned sample of the glass was mechanically polished and coated with a thin (10—20 nm) gold layer to prevent charging during SEM/EDS analysis (see Figure 1).

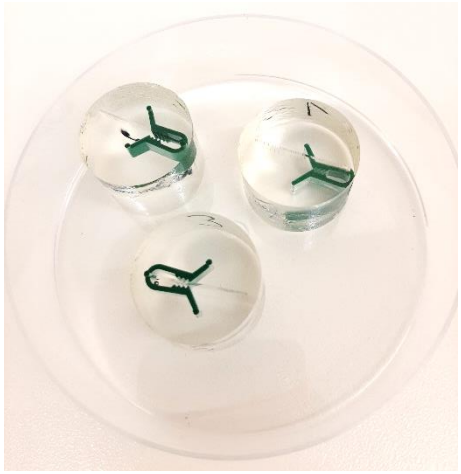

Figure 1. Glass samples (between green clamps) molded in epoxy and polished.

2.2. Picosecond laser inscribed artificial flaws

2.2.1. Laser system

The used irradiation source is a picosecond pulsed laser (Duetto, Time-Bandwidth Products), with a wavelength of 532 nm, a pulse duration less than 12 ps, and a pulse repetition rate of 50 kHz. Pulse energies up to 200 μJ and corresponding average power 10—15 W can be achieved. The laser setup is schematically depicted in Figure 2. The glass specimens were fixed on the translation stage with a vacuum chuck. A camera was used to visually locate the glass specimen on the table so that ablation can be performed at the desired location on the specimen, as illustrated in Figure 3. A galvanometer scanner enabled to control the speed of inscribing the artificial flaws. The laser was focused on the glass surface with an F-theta focusing lens of focal length 163 mm. Regarding the laser parameters, pulse energies up to 55.4 μJ, number of passes up to 60, and scan speeds of 200 mm/s were tested.

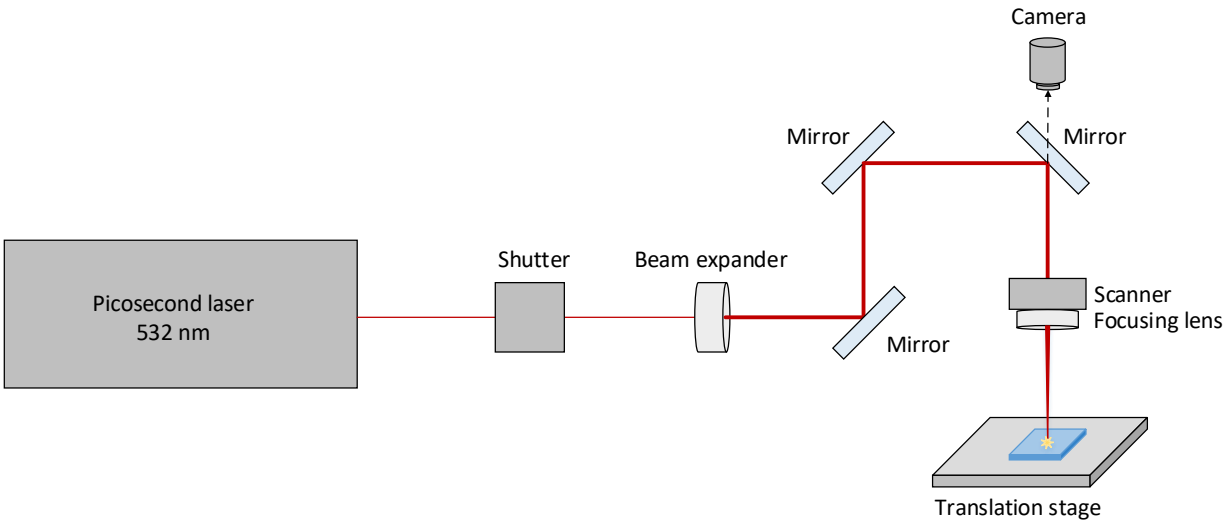

Figure 2. Schematic of picosecond laser setup.

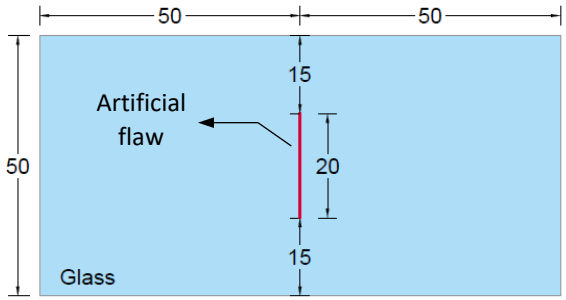

Figure 3. Schematic of glass specimen with the artificial flaw inscribed in the center (red line) and parallel to the shortest glass edge. Dimensions are in mm.

2.2.2. Laser parameter optimization

To achieve artificial flaws with desirable depths and to avoid unwanted cracks and chippings, laser ablation parameters were optimized on each glass type. A combination of pulse energy, translation speed, and the number of passes were investigated (Nategh et al. 2021a). It was admitted that the translation speed of 200 mm/s could yield acceptable flaws without lateral/median cracks and

chippings (assuming that the pulse energy is in a proper range). By fixing the speed, only two parameters of pulse energy and the number of passes were considered to control the flaw depth.

2.4. Flaws' depth measurement

To correlate the laser parameters to the flaw's depth, precise depth measurement is necessary. In this regard, many artificial flaws with different parameters were produced next to each other on each glass type. Afterward, the glass was diced through the center and perpendicular to the flaws using a dicing machine (DISCO DAD322) equipped with a diamond-coated blade. It was observed that the strengthened glass is more sensitive to any surface modifications and could break from various locations if the dicing parameters were not properly chosen. Therefore, a step-wise dicing technique with 1 mm/s speed and two passes, each time 300 μm blade penetration, was used to limit stress concentration during the dicing process. It should also be noted that this kind of technique for providing stress relaxation is more important for the case of CGS 24h compared with CSG 8h.

The diced pieces were subsequently polished to allow cross-sectional inspection. Therefore, each glass piece containing several flaws was molded in epoxy resin (XF40 and hardener XH40). After 12 hours of curing time at 25 ˚C, first grinding and then careful polishing was performed to prevent any damage to the area of interest. Between each grinding/polishing step, a thorough rinsing to flush debris particles from the sample was done and as a final cleaning step, the cross-sections are wiped with isopropyl alcohol. For measuring the ablation depth, an optical microscope (Nikon Eclipse LV100) is utilized.

2.3. Clamp bender

For the strength measurement, a clamp bender setup developed by AGC was used (see Figure 4) to apply a bending moment to the glass specimen's whole surface, excluding the small zone at the straight edges where the bending moment is introduced (Zaccaria et al. 2022). Therefore, the glass pieces were fixed from the sides to two arms with a width of 4 mm and a length of 80 mm on each side. During testing, both arms were rotated simultaneously, while the left arm had a linear motion towards the other arm to keep the bending moment constant and uniform. The tests are performed at a temperature of 20.5 ˚C ± 0.2 ˚C and relative humidity of 33.5% ± 4%.

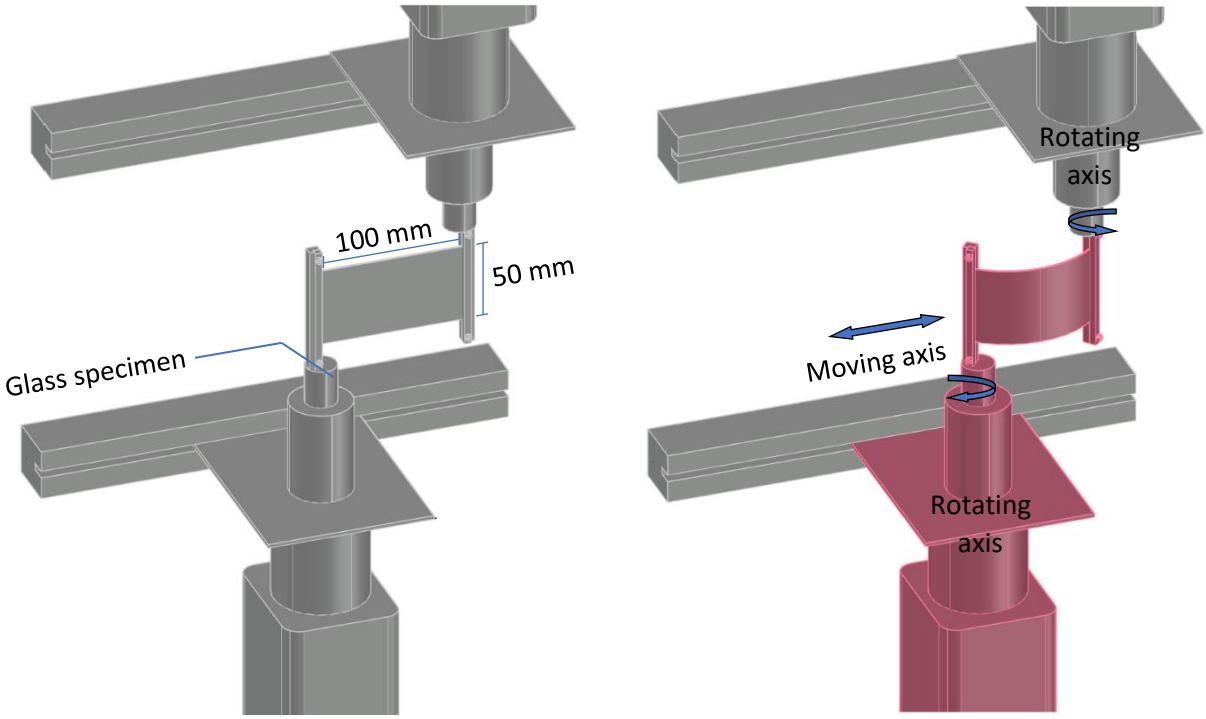

Figure 4. Schematic view of the clamp bender setup (red is the deformed state).

3. Results and discussion

3.1. Pre-stress and DoL measurement

The depth of layer (DoL) and surface compressive stress (C_S) are measured with a FSM-7000H (Orihara Industrial Co., Ltd) tool on both the air side and tin side of glasses type 1 and type 2. Five glass specimens were used for DoL and C_S measurements and for each piece, three random measurement locations were chosen. The results of the measurements are given in Table 1. The difference between the average values for the air-side and tin-side is mainly because of the tool accuracy (stress: ±20 MPa and depth: ±5 μm).

Since the glass was cut to size with a precise laser filamentation technique, length and width were relatively precise (100*50*0.5 ± 0.05 mm). However, the thickness of each specimen was measured at two points towards the corners using a digital thickness gauge and the average value was chosen for the strength calculations.

Table 1. Measured properties of the chemically toughened glass used (average values).

Glass	Air side		Tin side	
	DoL (μm)	C_s (MPa)	DoL (μm)	C_s (MPa)
CT-24h	78 ± 1	380 ± 7	81.5 ± 1	396 ± 8
CT-8h	47.5 ± 0.5	478 ± 10	47.5 ± 0.5	472 ± 7

3.2. SEM/EDS analysis

As mentioned before, a cross-sectioned sample of the glass needs to be mechanically polished before the EDS analysis (see Figure 5). Table 2 presents the glass composition for two spots resulting from the EDS analysis, in which spot 1 was very close the glass surface and spot 2 was at the depth of 112 μm below the surface. The main difference in the composition is related to Na^+ and K^+. For the case of pre-stressed glass (24h and 8h processing durations), concentration of K^+ is higher in spot 1 while concentration of Na^+ is higher in spot 2. This clearly implies that Na^+ is

replaced by K^+ close to the surface due to the ion-exchange process. Since 112 μm is deeper than the DoL (80 μm and 47.5 μm), the amount of K^+ in spot 2 is equal to that of the non-strengthened glass in both spots.

Figure 6 illustrates the SEM/EDS line scan results for all three glass types. As it can be seen, the exchange of K^+ from the salt bath with the Na^+ from the glass starts from the glass surface and continues until a certain depth (DoL) depending on the processing duration. The trendline indicates that the K^+ decreases almost parabolically to a certain value and then remains constant. Figure 6 (top) is the result of 24h processing in which the K^+ penetration is 79 ± 3 μm. This can also be considered as a verification of the DoL measured by the FSM-7000H tool (see Table 1). The same trend can be observed in Figure 6 (middle) for the case of 8h processing in which the DoL is 48 ± 3 μm. In Figure 6 (bottom), there is no sign of ion-exchange as it is a non-strengthened glass.

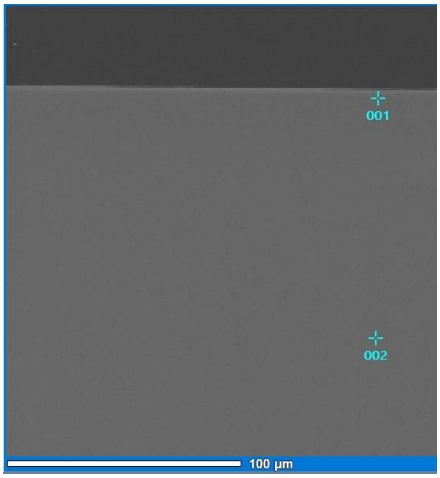

Figure 5. Location of spots 1 and 2 on the glass cross-section (SEM image).

Table 2. Estimated composition of the used aluminosilicate glass obtained using EDS. Spot 1 is very close to the glass surface and spot 2 is 112 μm below the surface.

Constituents	Proportion by mass of element (%)						Error (%)
	24h processing		8h processing		Non-strengthened		
	Spot 1	Spot 2	Spot 1	Spot 2	Spot 1	Spot 2	
Si	31.97	38.39	31.34	35.61	35.11	36.58	0.09
K	17.47	1.17	15.85	1.18	1.06	1.14	0.13
Na	2.52	10.43	3.18	10.00	11.02	10.95	0.14
Mg	5.72	6.35	5.44	6.43	6.23	6.36	0.11
Al	3.25	3.79	3.26	3.54	3.64	3.64	0.10
Others	< 1						

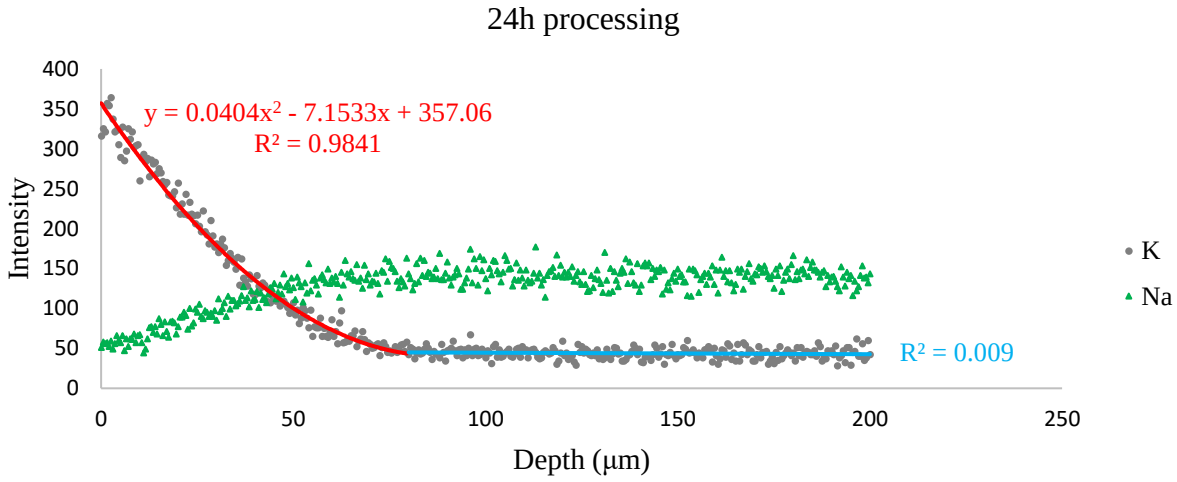

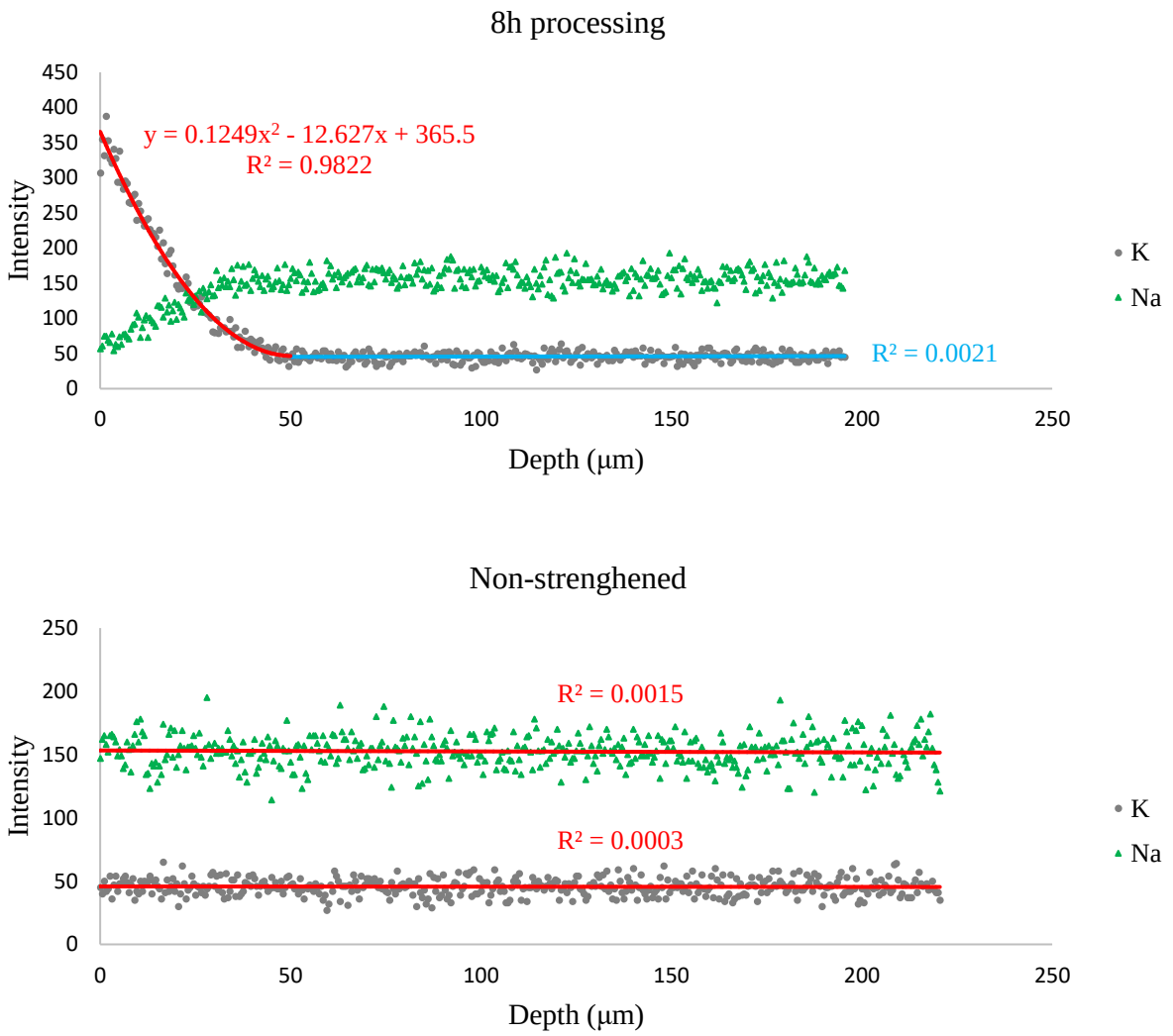

Figure 6. Distribution of K^+ and Na^+ using SEM/EDS analysis for 24h processing (top), 8h processing (middle), and non-strengthened (bottom) glasses.

3.3. Pre-stress distribution

There are several methods for determining the pre-stress distribution such as the scattered light method and RGB photoelasticity (Dix, Schuler and Kolling 2022; Laurs et al. 2019). The second-degree polynomial distribution was assumed for thermally toughened glass in which the pre-stress is produced by quenching of hot glass (Nielsen et al. 2021). Here, we assumed a pre-stress distribution according to the distribution of K^+, derived from the EDS analysis because the presence

of higher concentration of K^+ is the reason for such stress distribution in the glass. Although linear (Wang, Suo, and Manes 2021) and exponential (Macrelli et al. 2020) distributions were used in some literature, the second-degree polynomial function assumption according to the trendlines of Figure 6 is considered here. Another assumption is that the possible pre-stress peak movement due to stress relaxation (Sane and Cooper 1987; Seaman et al. 2014) during processing in the molten salt bath is neglected. Therefore, the following format can be followed.

$$\sigma(z) = az^2 + bz + c \tag{1}$$

To derive the pre-stress profile, the following boundary conditions can be used (see Figure 7).

$$\sigma(z = 0) = C_s \tag{2}$$

$$\sigma(z = DoL) = 0 \tag{3}$$

$$\sigma(z = d_t + DoL) = T_s \tag{4}$$

$$\left.\frac{d\sigma(z)}{dz}\right|_{z=d_t+DoL} = 0 \tag{5}$$

in which C_s is compressive pre-stress. T_s and d_t are tensile stress and its depth, respectively. Another equation comes from the pre-stress equilibrium in the glass:

$$\int_0^t \sigma(z)dz = 0 \tag{6}$$

Assuming that the difference in the compressive stress on the air side and the tin side is negligible (see Table 1), the rule of symmetry can be governed to Eq. 6 as follows

$$\int_0^{t/2} \sigma(z)dz = 0 \tag{7}$$

With these equations and by using C_s and DoL from Table 1 (measured experimentally), we can derive the pre-stress profile (assuming a symmetrical shape) and calculate T_s and d_t accordingly:

24h processing ($C_s = 390$ MPa, $DoL = 80$ µm):

$$\begin{aligned} &\sigma(z) = 24040.9\,(z - 0.14139)^2 - 90.6033; && 0 < z < 0.14139 \\ &\sigma(z) = -90.6033; && 0.14139 < z < 0.25 \\ &T_s = -90.6 \text{ MPa}, \quad d_t = 61.4\ \mu\text{m} \end{aligned} \tag{8}$$

8h processing ($C_s = 475$ MPa, $DoL = 47.5$ µm):

$$\begin{aligned} &\sigma(z) = 113109\,(z - 0.067955)^2 - 47.3264; && 0 < z < 0.067955 \\ &\sigma(z) = -90.6033; && 0.067955 < z < 0.25 \\ &T_s = -47.3 \text{ MPa}, \quad d_t = 20.5\ \mu\text{m}; \end{aligned} \tag{9}$$

The signs + and - indicate areas with compressive and tensile stresses, respectively. The pre-stress profiles derived from equations (8) and (9) are plotted in Figure 8.

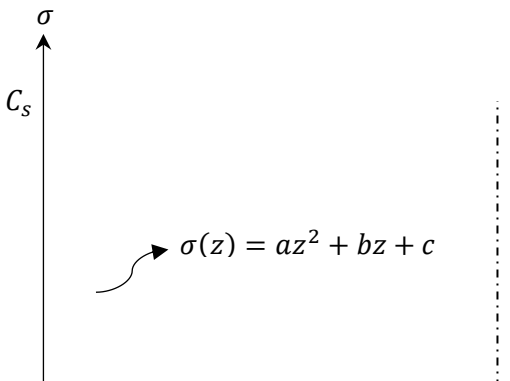

Figure 7. Pre-stress distribution over the thickness of chemically strengthened glass by assuming a second-degree polynomial distribution. The signs + and − indicate areas with compressive and tensile stresses, respectively.

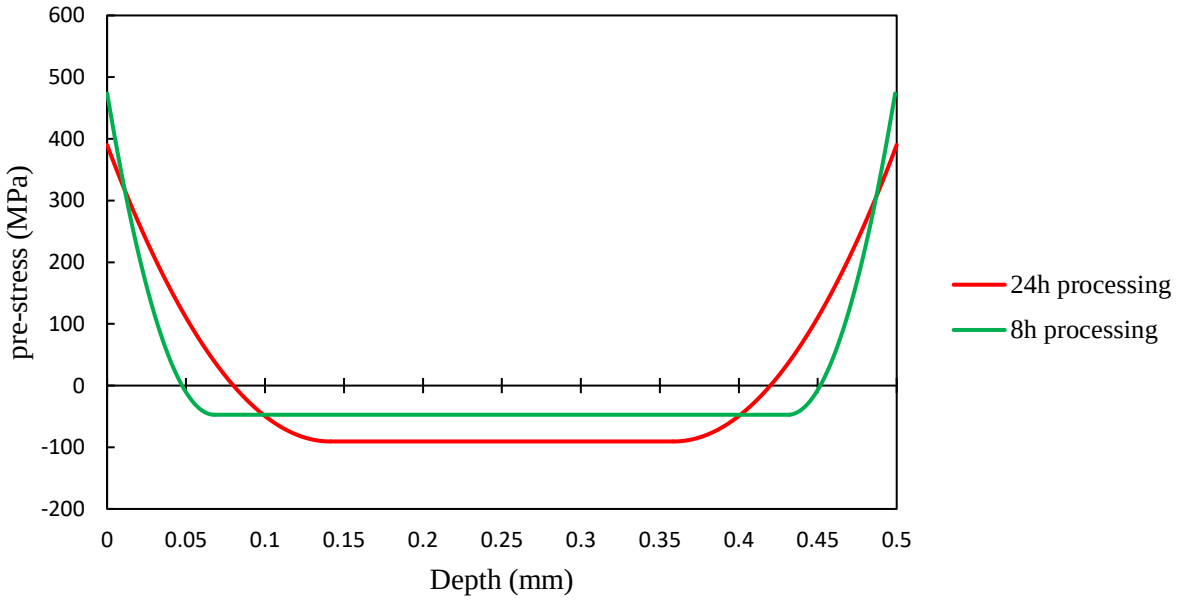

Figure 8. Pre-stress profiles for 24h and 8h processing durations, calculated based on the second-degree polynomial function assumption.

3.4. Artificial flaws

During the laser parameter optimization, it was found that generating artificial flaw of chemically toughened glass is more challenging than annealed glass. For example, for a pulse energy of 82 μJ and translation speed of 200 mm/s, the chemically toughened glass with 24h processing failed during the laser process while the glass with 8h processing stayed intact. This means that increasing the processing time makes the glass more vulnerable to failure upon crack generation, although its DoL is higher, indicating that the failure was induced by the stress distribution during flaw generation. The reason for this phenomenon is the amount of energy stored in CSG, which is higher for the case of 24h processing (see section 3.6). However, it does not imply that glass with 8h processing is necessarily stronger than glass with 24h processing, since theoretically, a larger DoL decreases the chance a crack exceeds the pre-compression layer, which can therefore be considered to be a safe region resisting crack propagation.

By optimizing the laser pulse energy with the goal of minimum failure during ablation, artificial flaws with three different depths were created on each glass type. Here the aim was having three depths: a) more than the DoL of CSG 24h, b) between the DoL of CSG 8h and CSG 24h, and c) less than DoL of CSG 8h. The measured artificial flaw depths obtained with the corresponding laser parameters are given in Table 3. Measured depth values resulted from microscopic cross-

sectional inspection of 10 identical flaws written next to each other. Figure 9 displays the microscopic images of one flaw from each category.

Table 3. Flaw characteristics and corresponding laser parameters.

Flaws characteristics				Laser parameters		
Flaw category	Specimens category	Flaw's depth (μm)	Standard deviations (μm)	Pulse energy (μJ)	Translation speed (mm/s)	Number of passes
Flaw A	CSG 24h-A	96.5	1.2	55.4	200	60
	CSG 8h-A	96.9	1			
	NSG-A	99.1	1.8			
Flaw B	CSG 24h-B	61.2	0.9	55.4	200	14
	CSG 8h-B	59.7	0.9			
	NSG-B	59.8	0.9			
Flaw C	CSG 24h-B	18.4	0.7	27.6	200	4
	CSG 8h-B	17.9	0.6			
	NSG-B	18.9	0.7			

Although the dominant ablation process for a picosecond laser is breaking the atomic bonds, some local heating followed by stress relaxation of the glass is inevitable. Here, this thermal effect was limited by decreasing the pulse energy and increasing the scan speed simultaneously. The lack of radial/median cracks and chippings was proved by microscopic inspection. The strength test showed limited stress relaxation that did not change the strengthened glass general behavior.

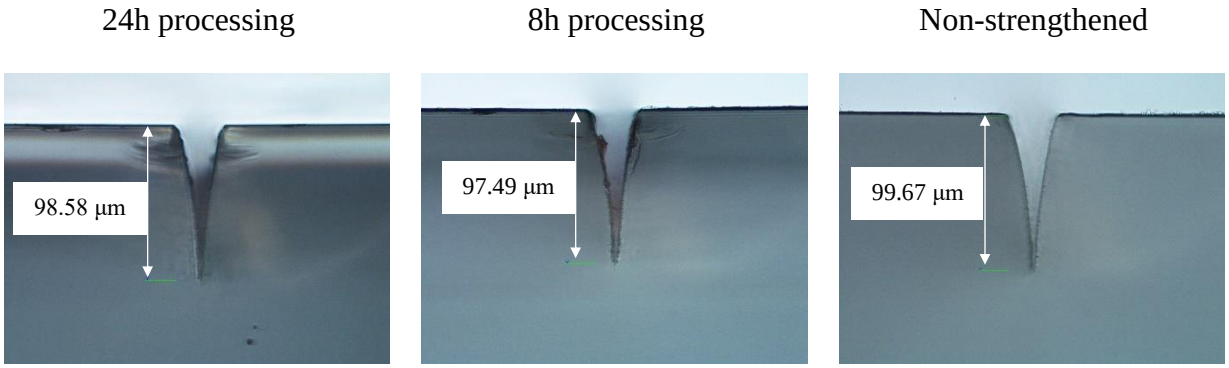

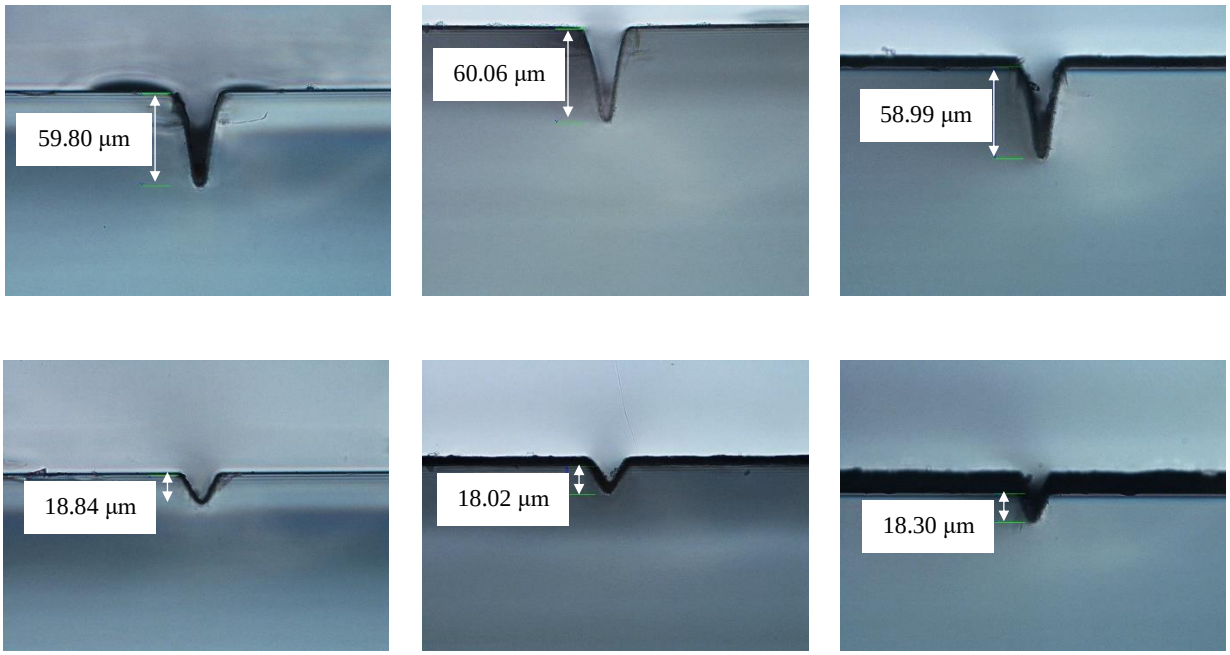

Figure 9. Artificial flaws geometries for 24h strengthening (left), 8h strengthening (middle), and non-strengthened (right) glasses.

3.5. Strength test

Glass with three different strengthening conditions and the three chosen artificial flaw depths (see Table 3) was tested on the clamp bending machine to understand the effect of surface flaw depth on the strength of chemically pre-stress glass with known DoL (see Table 1). Figure 10 plots the average strength values of 11 specimens for each category. The first observation is that the flaw depth has a direct impact on the strength values in such a way that the deeper is the flaw, the lower is the strength. The reason for not visualizing in a Weibull plot is the low standard deviations of the strength values. Essentially, we are not dealing with a probability distribution since the observed dispersions are (extremely) low for glass.

To examine the strengthening effect, the result of CSG 24h and the NSG can be compared. Figure 11 shows the pre-stress value with respect to the tip of each flaw category. For specimens with a flaw A (96-99 μm depth), CSG 24h has a strength value 120% higher than that of the NSG. Considering the DoL of 78-81um for CSG 24h, it can be concluded that strengthening improved the glass strength significantly even for flaws deeper than the DoL. It should be noted that when the flaw depth is larger than the DoL, the flaw tip is in the tensile region of the stress profile, which means that the glass is experiencing tensile stress willing to open the flaw. However, since the flaw is in the middle region of the glass (see Figure 3), the surrounding glass with compressive pre-stress resists failure. For flaw B (59-61 μm depth), CSG 24h has a strength value 179% higher than the strength of NSG. In this case, the flaw tip is still in the compressive pre-stress zone and taking advantage of its stress, which adds to the resistance of the surrounding glass. The trend indicates that strengthening is more effective on shallower flaws, but it still increases the glass strength for flaws deeper than the DoL. For flaw C (18-19 um depth), the strength values of CSG 24h were not reliable because most of the samples failed from the edge and not the location of the artificial flaw.

Comparing the result of specimens with 24 and 8 hours strengthening demonstrates that CSG 24h specimens have an average strength value of 13.5% and 30% higher than CSG 8h specimens for the flaw categories A and B, respectively. Considering the trend, CSG 24h seems more advantageous for the case of shallow flaws. The only exception is when the flaw is very superficial so that its depth is less than the depth corresponding to the intersection of 24h and 8h pre-stressing graphs (see Figure 11). Regarding flaw C, the standard deviations of strength values for CSG 8h are 18.4 MPa which is higher than usual (less than 2.5 MPa). The reason is that the failure of most of them originated from the edge and not from the artificial flaw. Therefore, the strength values

were not representative of samples with that specific flaw depth and were removed from the bar chart.

Although the dominant ablation process for a picosecond laser is breaking the atomic bonds, some local heating followed by stress relaxation of the glass is inevitable. Here, this thermal effect was limited by decreasing the pulse energy and increasing the scan speed simultaneously. The lack of radial/median cracks and chippings was proved by microscopic inspection. The strength test showed limited stress relaxation that did not change the strengthened glass general behavior.

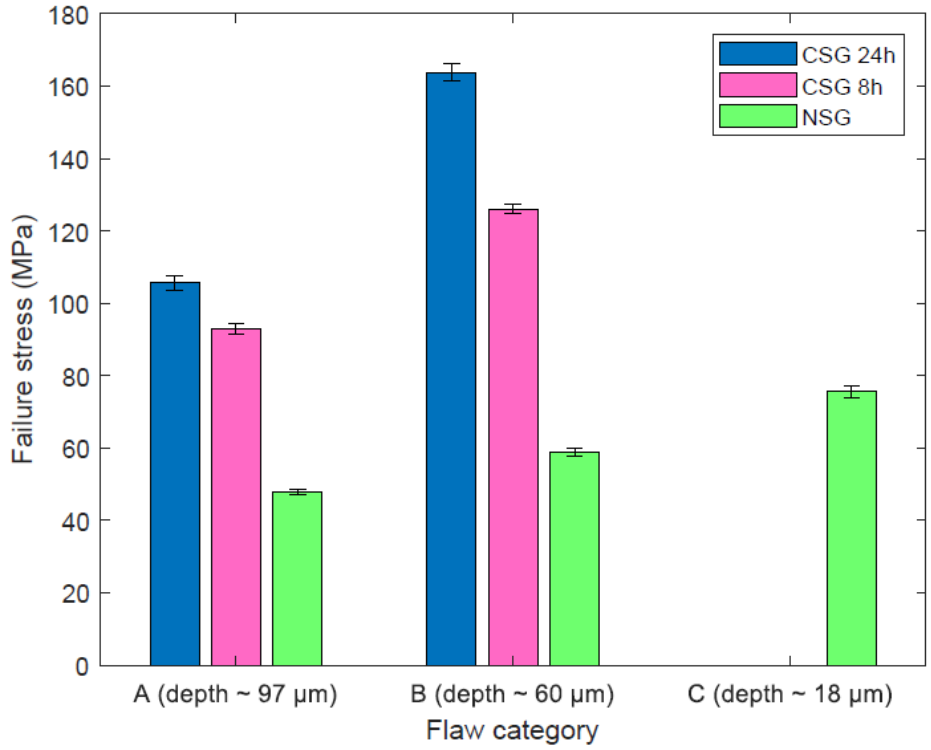

Figure 10. Average strength values corresponding to each flaw depth for specimens with different pre-stressing conditions.

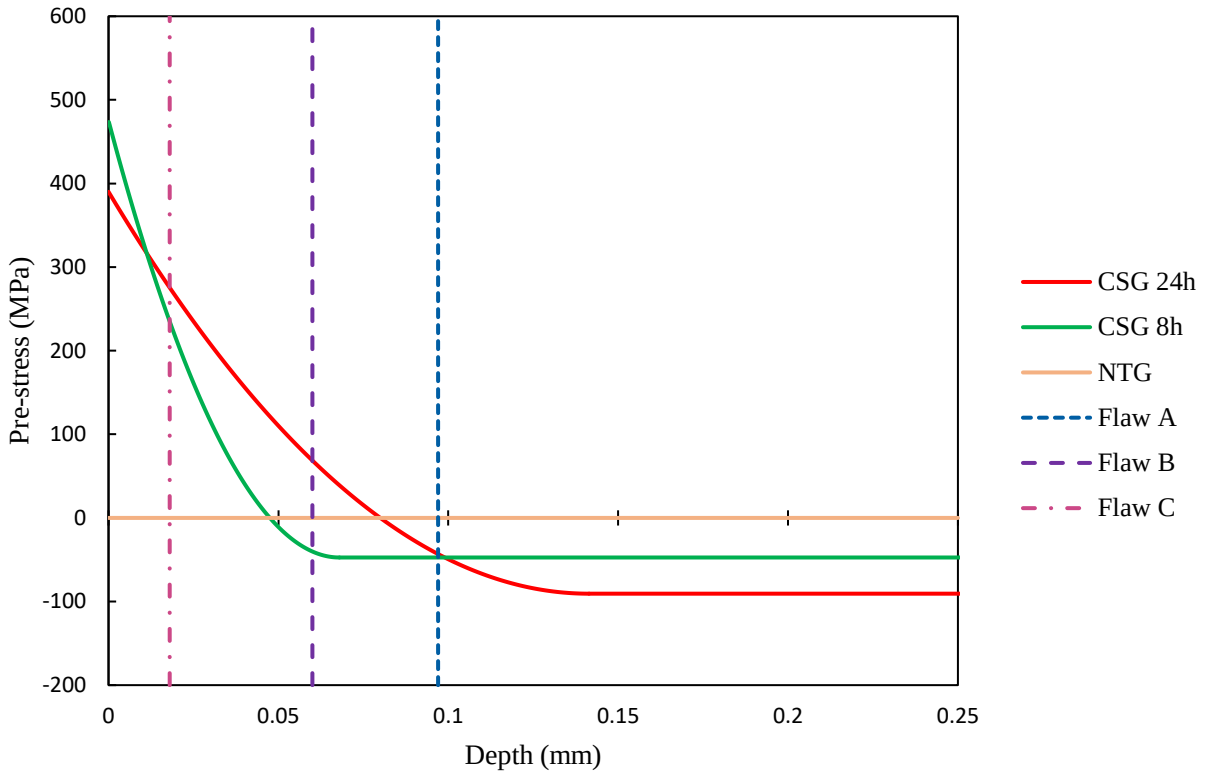

Figure 11. The pre-stress status with respect to the tip of each artificial flaw category.

3.6. Strain energy

Inspection of fracture patterns can help us to compare the energy stored in the CSG. One may say that the CSG 8h should have more energy because its compressive pre-stress (C_s) is higher (see Table 1). However, both C_s and DoL should be considered for calculating the energy. The strain energy in the CSG can be calculated as follows (Nielsen 2017):

$$U_{total} = U_{prestress} + U_{loading} \quad (10)$$

When the glass is not loaded, the existing energy is only due to the pre-stressing, leading to $U_{total} = U_{prestress}$.

To calculate the pre-stress strain energy under the assumption of a linear elastic behavior for the glass, the following equation can be written:

$$U_{pre-stress} = \frac{1}{2}\int_V \sigma_{ij}\varepsilon_{ij}dV \xrightarrow{Hooke's\ law} \frac{1-\nu}{E}\int_V \sigma^2 dV \tag{11}$$

In cylindrical coordiantes: $\frac{1-\nu}{E}\int_z\int_0^R\int_0^{2\pi}\sigma^2 r dr d\theta dz$

where V is the domain (volume) of the fragment considered, σ_{ij} and ε_{ij} are the stress- and strain tensor, ν is Poisson's ratio, E is the modulus of elasticity, r and θ are polar coordinates. Inserting the pre-stress equation from (1) to (11) and integrating in cylindrical coordinates, we can find the pre-stress strain energy per unit surface area (πR^2) for the investigated CSGs as follows ($\nu = 0.23$, $E = 70000$ MPa):

24h processing: $U_{pre-stress} = 0.0811\ N/mm$ (12)

8h processing: $U_{pre-stress} = 0.0619\ N/mm$ (13)

This indicates that the release of the energy upon failure is higher for CSG 24h and accordingly, the fracture pattern of CSG 24h should be finer than CSG 8h for a similar crack. Figure 12 shows the fracture pattern of all glass types.

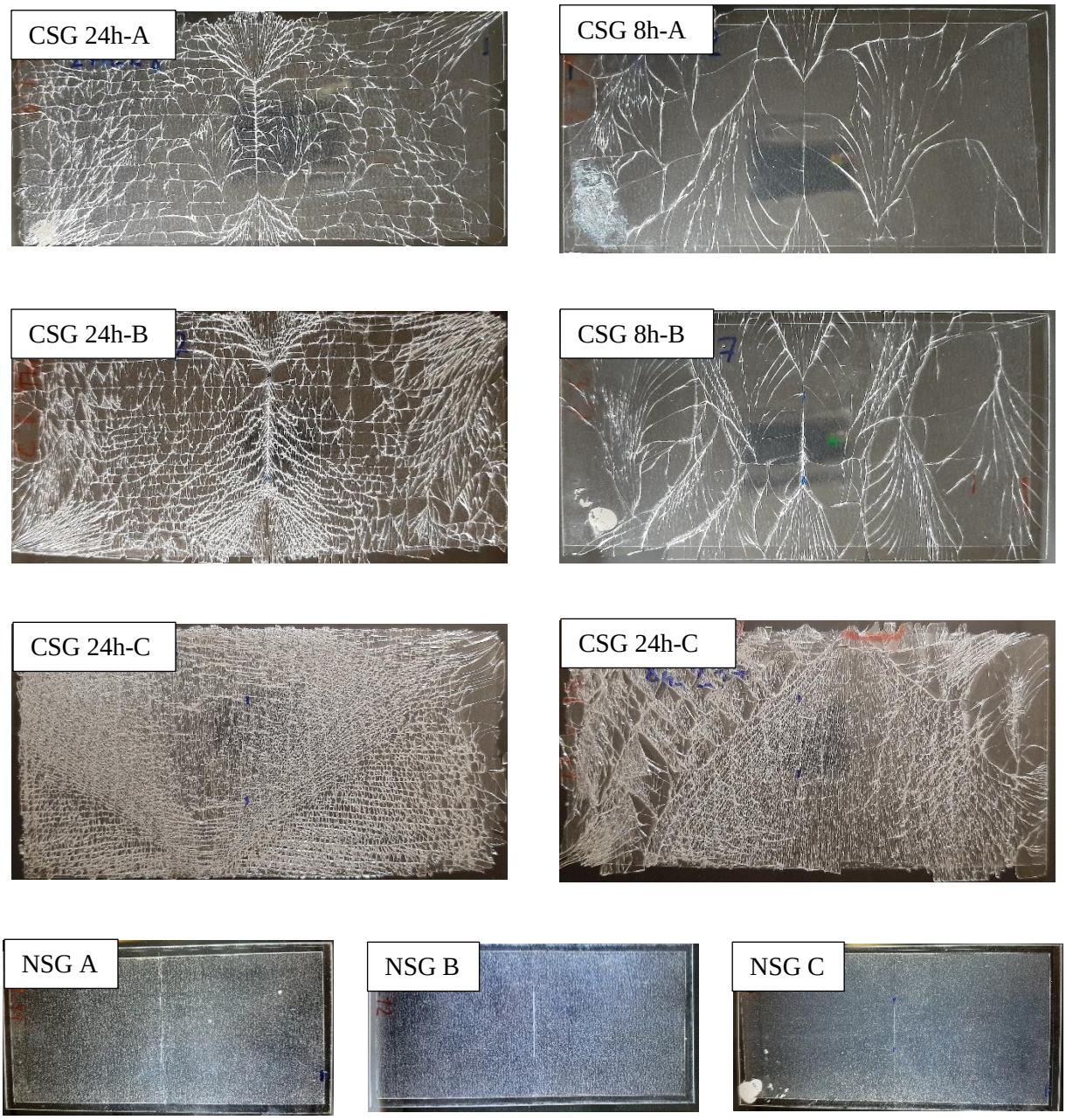

Figure 12. Fracture pattern of the different glass types (NSG, CSG 24h and CSG 8h) after the bending test for different flaw categories (A,B and C).

3.7. Fracture toughness

Fracture toughness is a material property independent of the size and geometry of the cracked body. Since we are able to generate identical flaws, it is relevant to investigate the effect of the pre-stressing process on the glass toughness. The following relation gives the fracture toughness of material for mode I loading:

$$K_{Ic} = Y\sigma_f\sqrt{\pi a} \tag{14}$$

where Y is the geometry factor of the crack, σ_f is the failure stress, and a is the crack depth. There are different parameters affecting Y such as length, shape, and sharpness of the artificial flaw (Tada, Paris, and Irwin 2010). Therefore, each flaw category is expected to have a unique geometry factor. The fracture toughness of the glass for each flaw category is given in Table 4, in which Y_A and Y_B are the geometry factors for the flaw categories A and B, respectively.

Since the artificial flaw geometry is identical for each category (see Figure 9), the only variable parameter is the failure stress (σ_f). Therefore, the change in the fracture toughness as a result of pre-stressing can be calculated as follows:

$$\frac{K_{Ic\,(CTG)}}{K_{Ic\,(NSG)}} = \frac{\sigma_{f\,CTG}}{\sigma_{f\,NSG}} \tag{15}$$

The ratio is then the same increase obtained in section 3.5. We can conclude that the fracture toughness changes through the glass thickness by varying the pre-stress value. The maximum toughness is on the glass surface where the pre-stress is maximum.

Table 4. Fracture toughness for 24h, 8h, and non-strengthened glasses.

	K_{Ic}	
Glass	Flaw A	Flaw B
CSG 24h	1.84 Y_A	2.27 Y_B
CSG 8h	1.62 Y_A	1.73 Y_B
NSG	0.85 Y_A	0.81 Y_B

4. Conclusions

This paper investigates the thin chemically pre-stressed glass (Falcon®) with two different processing durations (24h and 8h). A non-strengthened glass with the same composition is also used as a reference . It is inferred that by assuming the pre-stress profile follows the same trend as the K distribution through the glass thickness, which with a good approximation is a second-degree polynomial function obtained from the SEM/EDS analysis, we could obtain the pre-stress profile. However, the pre-compression value is required for this purpose, which can be easily measured by FSM-7000h. The DoL can be either measured by FSM-7000h or by SEM/EDS analysis. Both methods gave the same result, but FSM-7000h seems more straightforward.

Regarding the strength of pre-stressed glasses having three types of artificial flaws with depths of around 18 μm, 60 μm, and 97 μm, results showed that even when the depth of flaw is higher than the DoL, which means that the flaw tip enters the zone with the tensile pre-stress, there is still considerable resistance from the surrounding intact area. For example, for the DoL of around 80 μm for 24h CSG, the strength is 120% and 179% higher than the strength of NSG when the flaw depth is 97 μm and 60 μm, respectively.

To examine the different strengthening conditions, 24h and 8h, same surface flaws were created. Having an average strength value of 13.5% and 30% higher than CSG 8h specimens for the flaw categories A and B, CSG 24h generally seems more advantageous for the case of shallow flaws.

The only exception is when the flaw is very superficial so that its depth is less than the depth corresponding to the intersection of 24h and 8h pre-stressing profiles. The reason is that the pre-stress value at the surface is higher for 8h strengthening. Therefore, when the flaw tip is very close to the surface, the pre-stress value is still very high. However, this value drops faster for the case of 8h strengthening compared with 24h strengthening. On the other hand, the situation is different when the flaw is deep enough to reach the tensile zone of 24h pre-stressed glass since the tensile pre-stress is higher.

Furthermore, it is pointed out that the pre-stress strain energy for 24h strengthening is larger than for 8h strengthening, leading to more fragmentation after failure under a similar loading condition. Finally, it was found that the fracture toughness is not constant through the CSG thickness, and it is dependent on the pre-stress profile with the peak value at the glass surface.

Declaration

Conflict of interest On behalf of all authors, the corresponding author states that there is no conflict of interest.

Acknowledgements

The authors gratefully acknowledge the support of AGC in providing thin glass samples and the strength testing setup for this study. Furthermore, the authors would like to acknowledge the support of technicians in the Cleanroom (associated imec laboratory at Ghent University) and Magnel-Vandepitte laboratory, Department of Structural Engineering and Building Materials of Ghent University.

References

"ASTM C1499-19, Standard Test Method for Monotonic Equibiaxial Flexural Strength of Advanced Ceramics at Ambient Temperature, ASTM International, West Conshohocken, PA." 2019. https://doi.org/10.1520/C1499-19.

"ASTM C158-02(2017), Standard Test Methods for Strength of Glass by Flexure (Determination of Modulus of Rupture), ASTM International, West Conshohocken, PA." 2017. https://doi.org/10.1520/C0158-02R17.

Bartenev, G. 1948. "The Phenomenon of the Hardening of Glass." *J Tech Phys* 18: 383–88.

Belis, Jan, Christian Louter, Jens H Nielsen, and Jens Schneider. 2019. "Architectural Glass." In *Springer Handbook of Glass*, edited by J David Musgraves, Juejun Hu, and Laurent Calvez, 1781–1819. Cham: Springer International Publishing. https://doi.org/10.1007/978-3-319-93728-1_52.

Bensaid, Nasreddine, Saci Benbahouche, Fouad Roumili, Jean Christophe Sangleboeuf, Jean Benoît Le Cam, and Tanguy Rouxel. 2018. "Influence of the Normal Load of Scratching on Cracking and Mechanical Strength of Soda-Lime-Silica Glass." *Journal of Non-Crystalline Solids*. https://doi.org/10.1016/j.jnoncrysol.2018.01.004.

Dix, Steffen, Christian Schuler, and Stefan Kolling. 2022. "Digital Full-Field Photoelasticity of Tempered Architectural Glass: A Review." *Optics and Lasers in Engineering* 153 (September 2021): 106998. https://doi.org/10.1016/j.optlaseng.2022.106998.

"EN 1288-2, Glass in Building - Determination of Bending Strength of Glass - Part 2: Coaxial Double Ring Test on Flat Specimens with Large Test Surface Areas." 2000.

"EN 1288-3, Glass in Building - Determination of the Bending Strength of Glass - Part 3: Test with Specimen Supported at Two Points (Four Point Bending)." 2000.

"EN 1288-5, Glass in Building - Determination of the Bending Strength of Glass - Part 5: Coaxial Double

Ring Test on Flat Specimens with Small Test Surface Areas." 2000.

Glaesemann, G. Scott, Karl Jakus, and John E. Ritter. 1987. "Strength Variability of Indented Soda-Lime Glass." *Journal of the American Ceramic Society* 70 (6): 441–44. https://doi.org/10.1111/j.1151-2916.1987.tb05665.x.

Gy, René. 2008. "Ion Exchange for Glass Strengthening." *Materials Science and Engineering B: Solid-State Materials for Advanced Technology* 149 (2): 159–65. https://doi.org/10.1016/j.mseb.2007.11.029.

Jiang, Liangbao, Xintao Guo, Xiaoyu Li, Lei Li, Guanli Zhang, and Yue Yan. 2013. "Different K + -Na + Inter-Diffusion Kinetics between the Air Side and Tin Side of an Ion-Exchanged Float Aluminosilicate Glass." *Applied Surface Science* 265: 889–94. https://doi.org/10.1016/j.apsusc.2012.11.143.

Karlsson, Stefan, Bo Jonson, and Christina Stålhandske. 2010. "The Technology of Chemical Glass Strengthening-a Review." *Glass Technology* 51 (2): 41–54.

Kistler, S S. 1962. "Stresses in Glass Produced by Nonuniform Exchange of Monovalent Ions." *Journal of the American Ceramic Society* 45 (2): 59–68. https://doi.org/https://doi.org/10.1111/j.1151-2916.1962.tb11081.x.

Laurs, Maximilian, Benjamin Schaaf, Pietro Di Biase, and Markus Feldmann. 2019. "Determination of Prestress Profiles in Chemically Toughened Glass by Means of Photoelasticity." In *GPD Glass Performance Days*, 145–49.

Lee, E H, T G Rogers, and T C Woo. 1965. "Residual Stresses in a Glass Plate Cooled Symmetrically from Both Surfaces." *Journal of the American Ceramic Society* 48 (9): 480–87. https://doi.org/https://doi.org/10.1111/j.1151-2916.1965.tb14805.x.

Macrelli, Guglielmo. 2018. "Chemically Strengthened Glass by Ion Exchange: Strength Evaluation." *International Journal of Applied Glass Science* 9 (2): 156–66. https://doi.org/10.1111/ijag.12291.

Macrelli, Guglielmo, Nahide Özben, Ahmet Caner Kayaalp, Miray Çelikbilek Ersundu, and İlkay Sökmen.

2020. “Stress in Ion Exchanged Soda-Lime Silicate and Sodium Aluminosilicate Glasses: Experimental and Theoretical Comparison.” *International Journal of Applied Glass Science* 11 (4): 730–42. https://doi.org/10.1111/ijag.15787.

Maniatis, Iris, Gordon Nehring, and Geralt Siebert. 2016. “Studies on Determining the Bending Strength of Thin Glass.” *Proceedings of the Institution of Civil Engineers: Structures and Buildings* 169 (6): 393–402. https://doi.org/10.1680/jstbu.14.00003.

Moayedi, Elham, and Lothar Wondraczek. 2017. “Quantitative Analysis of Scratch-Induced Microabrasion on Silica Glass.” *Journal of Non-Crystalline Solids*. https://doi.org/10.1016/j.jnoncrysol.2017.05.003.

Nategh, S., J. Missinne, P. Vijverman, G. Van Steenberge, and J. Belis. 2021a. “Effect of Ultrashort Laser-Induced Surface Flaws on Architectural Glass Strength.” *Construction and Building Materials* 295: 123590. https://doi.org/10.1016/j.conbuildmat.2021.123590.

Nategh, S., E. Symoens, J. Missinne, and J. Belis. 2021b. “Effect of Loading Rate, Surface Flaw Length and Orientation on Strength of Laser-Modified Architectural Glass.” In *IABSE Congress : Structural Engineering for Future Societal Needs*, 1581–88. https://doi.org/10.2749/ghent.2021.1581.

Neugebauer, J. 2016. “Determination of Bending Tensile Strength of Thin Glass.” *Challenging Glass Conference Proceedings - Challenging Glass 5: Conference on Architectural and Structural Applications of Glass, CGC 2016*, no. June: 419–28.

Nielsen, J. H. 2017. “Remaining Stress-State and Strain-Energy in Tempered Glass Fragments.” *Glass Structures and Engineering* 2 (1): 45–56. https://doi.org/10.1007/s40940-016-0036-z.

Nielsen, J. H., J. F. Olesen, and H. Stang. 2010. “Characterization of the Residual Stress State in Commercially Fully Toughened Glass.” *Journal of Materials in Civil Engineering* 22 (2): 179–85. https://doi.org/10.1061/(asce)0899-1561(2010)22:2(179).

Nielsen, J. H., K. Thiele, J. Schneider, and M. J. Meyland. 2021. “Compressive Zone Depth of Thermally

Tempered Glass." *Construction and Building Materials* 310 (July): 125238. https://doi.org/10.1016/j.conbuildmat.2021.125238.

Nordberg, Martin E., Ellen L. Mochel, Harmon M. Garfinkel, and Joseph S. Olcott. 1964. "Strengthening by Ion Exchange." *Journal of the American Ceramic Society* 47 (5): 215–19. https://doi.org/10.1111/j.1151-2916.1964.tb14399.x.

Sane, AJIT Y, and A R Cooper. 1987. "Stress Buildup and Relaxation During Ion Exchange Strengthening of Glass." *Journal of the American Ceramic Society* 70 (2): 86–89. https://doi.org/https://doi.org/10.1111/j.1151-2916.1987.tb04934.x.

Santos, Francisco Oliveira, Christian Louter, and João Ramôa Correia. 2018. "Exploring Thin Glass Strength Test Methodologies." In *Challenging Glass 6: Conference on Architectural and Structural Applications of Glass, CGC 2018 - Proceedings*. https://doi.org/10.7480/cgc.6.2192.

Schneider, J., S. Schula, and W. P. Weinhold. 2012. "Characterisation of the Scratch Resistance of Annealed and Tempered Architectural Glass." *Thin Solid Films* 520 (12): 4190–98. https://doi.org/10.1016/j.tsf.2011.04.104.

Schwind, Gregor, Fabian von Blücher, Michael Drass, and Jens Schneider. 2020. "Double Ring Bending Tests on Heat Pretreated Soda–Lime Silicate Glass." *Glass Structures and Engineering* 5 (3): 429–43. https://doi.org/10.1007/s40940-020-00129-3.

Seaman, J. H., P. J. Lezzi, T. A. Blanchet, and M. Tomozawa. 2014. "Degradation of Ion-Exchange Strengthened Glasses Due to Surface Stress Relaxation." *Journal of Non-Crystalline Solids* 403: 113–23. https://doi.org/10.1016/j.jnoncrysol.2014.07.016.

Tada, Hiroshi, Paul C. Paris, and George R. Irwin. 2010. *The Stress Analysis of Cracks Handbook, Third Edition*. *The Stress Analysis of Cracks Handbook, Third Edition*. https://doi.org/10.1115/1.801535.

Terakado, Nobuaki, Ryusei Sasaki, Yoshihiro Takahashi, Takumi Fujiwara, Shuji Orihara, and Yoshio

Orihara. 2020. “A Novel Method for Stress Evaluation in Chemically Strengthened Glass Based on Micro-Raman Spectroscopy.” *Communications Physics* 3 (1): 1–7. https://doi.org/10.1038/s42005-020-0305-7.

Tyagi, Vineet, and Arun K. Varshneya. 1998. “Measurement of Progressive Stress Buildup during Ion Exchange in Alkali Aluminosilicate Glass.” *Journal of Non-Crystalline Solids* 238 (3): 186–92. https://doi.org/10.1016/S0022-3093(98)00691-7.

Varshneya, Arun K., Guglielmo Macrelli, Satoshi Yoshida, Seong H. Kim, Andrew L. Ogrinc, and John C. Mauro. 2021. “Indentation and Abrasion in Glass Products: Lessons Learned and yet to Be Learned.” *International Journal of Applied Glass Science*, no. October 2021: 1–30. https://doi.org/10.1111/ijag.16549.

Wang, Zhen, Tao Suo, and Andrea Manes. 2021. “Effect of Chemical Strengthening Residual Stress on the Flexural Performance and Fracture Behavior of Aluminosilicate Glass.” *Engineering Fracture Mechanics* 258 (November): 108104. https://doi.org/10.1016/j.engfracmech.2021.108104.

Zaccaria, Marco, Michel Dubru, Nerio Lucca, and Anna Šikyňová. 2021. “Chemically Strengthened Glass for Architectural Applications.” *Ce/Papers* 4 (6): 135–44. https://doi.org/10.1002/cepa.1626.

Zaccaria, Marco, and Mauro Overend. 2020. “Nondestructive Safety Evaluation of Thermally Tempered Glass.” *Journal of Materials in Civil Engineering* 32 (4): 04020043. https://doi.org/10.1061/(asce)mt.1943-5533.0003086.

Zaccaria, Marco, Timon Peters, Jan Ebert, Nerio Lucca, Jens Schneider, and Christian Louter. 2022. “The Clamp Bender: A New Testing Equipment for Thin Glass.” *Glass Structures & Engineering* 7 (2): 173–86. https://doi.org/10.1007/s40940-022-00188-8.